IEEE Photonics Journal
An IEEE Photonics Society Publication

Open Access

Rough Side-Polished Fiber With Surface Scratches for Sensing Applications

Volume 7, Number 3, June 2015

Jing Zhao
Guolu Yin
Changrui Liao
Shen Liu
Jun He
Bing Sun
Guanjun Wang
Xizheng Xu
Yiping Wang, Senior Member, IEEE

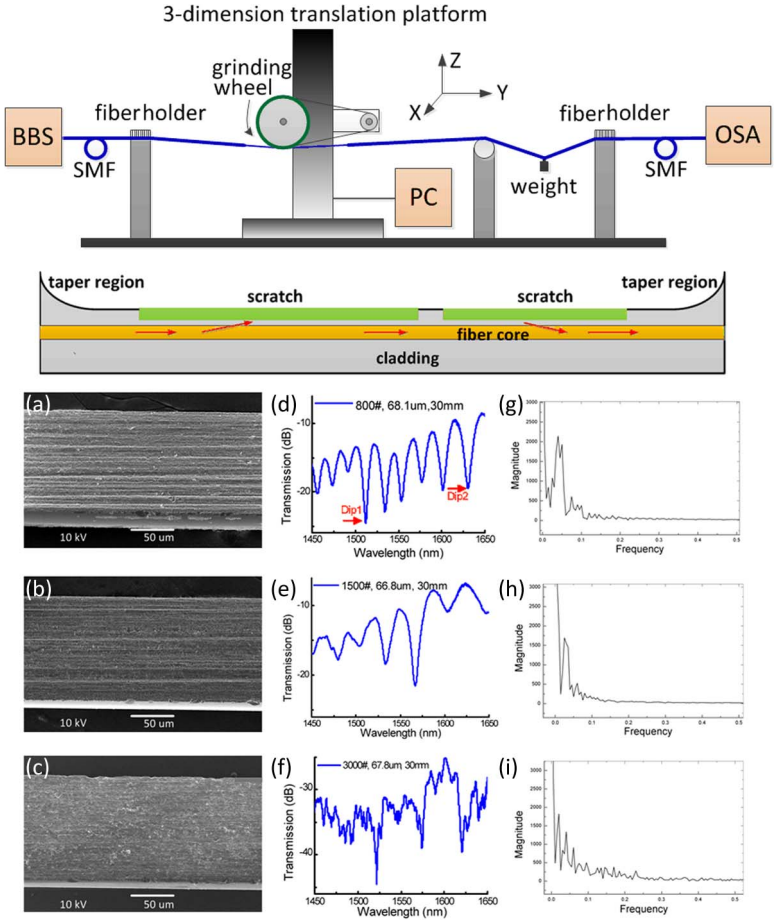

DOI: 10.1109/JPHOT.2015.2423288
1943-0655

Rough Side-Polished Fiber With Surface Scratches for Sensing Applications

Jing Zhao, Guolu Yin, Changrui Liao, Shen Liu, Jun He, Bing Sun, Guanjun Wang, Xizheng Xu, and Yiping Wang, *Senior Member, IEEE*

Key Laboratory of Optoelectronic Devices and Systems of Ministry of Education and Guangdong Province, College of Optoelectronic Engineering, Shenzhen University, Shenzhen 518060, China

DOI: 10.1109/JPHOT.2015.2423288

Manuscript received March 11, 2015; revised April 8, 2015; accepted April 10, 2015. Date of publication April 15, 2015; date of current version April 29, 2015. This work was supported in part by the National Natural Science Foundation of China under Grant 61425007, Grant 11174064, Grant 61377090, and Grant 61308027; by the Natural Science Foundation of Guangdong under Grant 2014A030308007 and Grant 2014A030312008; by the Science and Technology Innovation Commission of Shenzhen/Nanshan under Grant KQCX20120815161444632, Grant KC2014ZDZJ0008A, Grant JCYJ20130329140017262, and Grant ZDSYS20140430164957664; and by Pearl River Scholar Fellowships. Corresponding author: Y. Wang (e-mail: ypwang@szu.edu.cn).

Abstract: We demonstrated a fast mechanical wheel lapping technique to fabricate a convenient and low-cost side-polished fiber (SPF) with a rough, rather than smooth, polished surface. Such a bare SPF can be directly used to develop a promising sensing device, because a Mach–Zehnder interference pattern with high fringe contrast above 10 dB in transmission spectrum was achieved due to the macro scratches on the rough polished surface. Fabrication parameters, e.g., thickness of remaining fiber, polished length, and roughness of abrasive paper, were optimized. The sensor exhibited strain and temperature sensitivities up to -2.00 pm/$\mu\varepsilon$ and 29.37 pm/°C and can be used to realize simultaneous strain and temperature measurement.

Index Terms: Optical fiber sensors, side polished fiber, surface scratch, Mach–Zehnder interference.

1. Introduction

Side polished fiber (SPF) has been widely used in a variety of applications, including direction couplers, attenuators, polarizers, switches, resonators, filters, and evanescent fiber sensors, owing to the well-known evanescent field on the polished fiber surface [1]–[4]. Most of these components share a common fabrication process that a single mode fiber is glued by epoxy into a cutting curved V-shaped groove with its cladding polished away over a limited interaction length of several millimeters [5]. According to the fiber diameter and the remaining cladding thickness, different size of the V-shaped grooves have to be made precisely in advance by complicated techniques to achieve a desired SPF, which results in a low efficiency and a high cost. Alternatively, wheel polishing technique is more efficient by using a rolling wheel dressed with abrasive to polish fiber fixed on the flat surface. Since the V-shaped groove is not required, SPF with long interaction region can be realized flexibly by wheel polishing technique [6]. The distance from the polished surface to the fiber core, i.e., so-called remaining cladding thickness d, can be measured by liquid-drop method [7], [8]. Usually, a standard SPF fabrication begins with a rough lapping process by coarse abrasive and then is followed by a fine polishing process to remove the

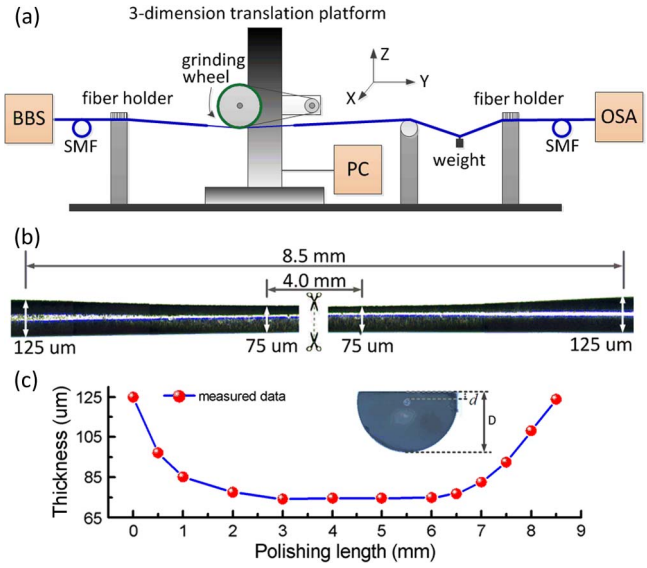

Fig. 1. (a) Schematic of the wheel polishing setup. (b) Microscope image of the achieved SPF. (c) Measured remaining thickness of the SPF along the whole polished region. The inset shows the cross section of the SPF where "*d*" and "*D*" are the remaining cladding and fiber thickness, respectively.

surface scratches. However, complicated post processing always takes a long time to create a high quality SPF with smooth surface, which is a bottleneck to the SPF's applications.

In this paper, we demonstrated a fast mechanical wheel lapping technique to fabricate a convenient and low cost SPF with a rough, rather than smooth, polished surface. Such a bare SPF exhibits clear interference fringes in transmission spectrum and can be used to develop promising fiber sensors, e.g., strain and temperature sensor. The scratches on the rough polished surface are the secret.

2. Experimental Details

As shown in Fig. 1(a), a wheel polishing setup (WanRun Ltd., WuXi, China) was employed to fabricate a SPF [9]. A cylinder grinding wheel was fastened on a precise 3-D translation platform that can be moved along the X, Y, and Z directions via computer control. Here, the wheel axis and the fiber axis were defined as the Z and Y direction, respectively. First, a standard SMF (Corning SMF-28) with a core/cladding diameter of 8.2/125 μm was fixed by a pair of fiber holders. A 20 g weight was hung to provide a constant tension to the polished fiber. The fiber coating was stripped in advance over a section of polished length and then cleaned by alcohol. Secondly, the coarse abrasive paper was winded and fastened around the wheel with paroline dropped onto the abrasive paper as lubrication. Thirdly, the wheel was drive down along the Z directions. Here, the rolling speed of the wheel and moving distance along the Y direction were preset in the computer. Then, the unjacketed fiber was gradually polished by the rolling wheel moving forth and back along the Y direction. During the polishing process, the side view of the SPF was monitored along the X direction by use of a microscope. Fig. 1(b) illustrates the side view of an achieved SPF. The remaining fiber thickness "*D*" of the SPF sample was measured along the whole polished region, as shown in Fig. 1(c). It can be found that the 8.5 mm-length SPF sample consists of a flat region with a length of about 4.0 mm and two tapered transition regions with a length of about 2 to 2.5 mm.

A broadband light source (BBS) light source with the range of 1250 nm to 1650 nm and an optical spectrum analyzer (OSA, YOKOGAWA AQ6370C) were employed to measure the transmission profile of SPF during the polishing process [10]. Coarse abrasive papers (800-mesh, 1500-mesh, 3000-mesh, Warriors 991A, STABCKE, Germany) were chosen to fabricated SPF

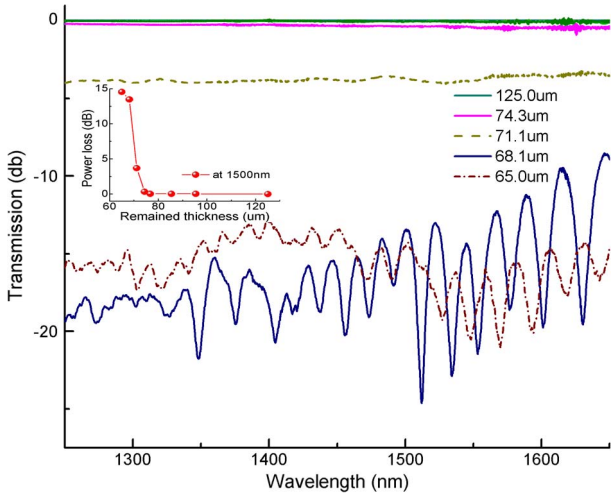

Fig. 2. Transmission spectrum evolution of 30.0 mm-length SPF fabricated by 800-mesh abrasive, when remaining fiber thickness "*D*" reduced from 125.0 μm to 65.0 μm.

samples with different surface roughness. The particle size of 800-mesh, 1500-mesh, and 3000-mesh abrasive was 19 μm, 10 μm, and 5 μm, respectively. After each lapping step, the polished surface was gently cleaned by an air-laid paper with alcohol to wipe off the residual silica dust and paroline. Noting that the position of polished surface cannot be changed to reduce the measurement error of "*D*," and the SPF needs to be always straightened naturally to avoid small bend perturbation.

3. Parameter Optimization

To investigate the influence of the remaining fiber thickness, the 800-mesh abrasive paper was employed to fabricate a rough SPF with polished length of 30 mm. Fig. 2 and the inset show the evolution of transmission profile and power loss during the whole lapping process. At early stage of the process, when remaining fiber thickness '*D*' stay above 75 μm (i.e., $d > 8$ μm), light was fully guided in the fiber core and the power loss can be ignored. As the polished depth increased continually, the power loss gradually increased first and then rose sharply with "*D*" reduced to less than 72 μm (i.e., $d < 5$ μm). While the SPF was lapped to near the core region, usually "*D*" was below 69 μm (i.e., $d < 2$ μm), interference pattern was observed in the transmission spectrum and the fringe contrast increased with the continual reduction of *d*. It could be considered as the interference between the core mode and the cladding modes induced by the surface scratches which will be analyzed in the following content. However, when the SPF was lapped into the fiber core, usually when "*D*" was less than 66 μm, (i.e., $d < -1$ μm), the fringe contrast gradually decreased due to the cutoff some cladding modes [11]. To achieve high contrast interference patterns, "*D*" was always controlled between 66 to 68 μm in fabrication.

To investigate the influence of surface roughness on the transmission spectrum, three samples, i.e., SPF1, SPF2, and SPF3, with the same polished length of 30 mm were fabricated by 800, 1500, and 3000-mesh coarse abrasive papers, respectively. The lapping process was stopped as soon as a relative high contrast fringe pattern was observed in the spectrum. Top views of the polished surface from three SPFs were observed by 500$\times$ SEM (JSM-5910LV, Scanning Electron Microscope, JEOL, Japan). Fig. 3(a) shows the polished surface of SPF1 fabricated by the 800-mesh abrasive paper, which is the roughest one with wide and deep macro scratches parallel to each other along the fiber axis. The polished surface of SPF2 shown in Fig. 3(b) is similar to SPF1 but the size of scratches is smaller. In contrast, SPF3 shown in Fig. 3(c) is the smoothest one with a relatively uniform surface without obvious macro scratches. Transmission profiles of SPF1and SPF2 are shown in Fig. 3(d) and (e). Sinusoid spectral profile with high fringe contrast above 10dB at maximum in the range of 1450 to 1650 nm was

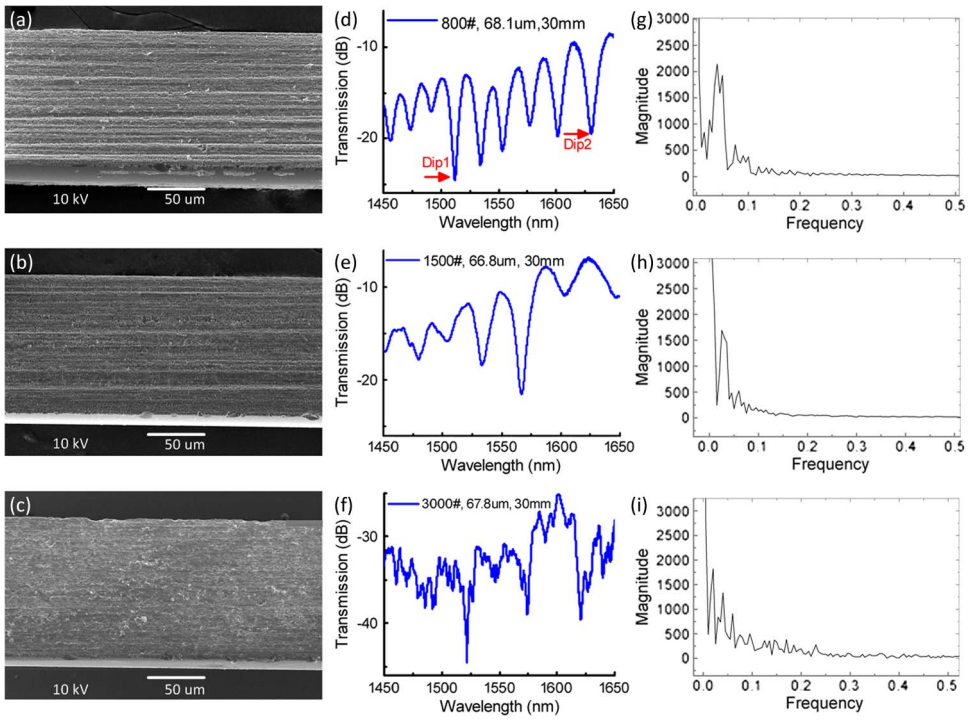

Fig. 3. Three samples SPF1, SPF2, and SPF3 were fabricated by 800, 1500, and 3000-mesh abrasive paper respectively. (a), (b), and (c) Top views of the polished surface of SPFs; (d), (e), and (f) their corresponding transmission spectra; and (g), (h), and (i) FFT analysis for three SPFs.

observed. Whereas for smoother SPF3 by fine 3000-mesh abrasive, the irregular interference pattern with higher insertion loss above 30 dB was observed in Fig. 3(f). FFT analysis of transmission spectrum was conduct. As shown in Fig. 3(i), it can be seen that multiple peaks existing in the FFT of SPF3, indicating that several cladding modes take part in the interference with the core mode. Whereas for FFT of SPF1 and SPF2 shown in Fig. 3(g) and (h), obviously only one main peak exist in FFT diagram, indicating that mainly one cladding mode engaged in the interference with the core mode, which agree with the sinusoid spectrum show in Fig. 3(d) and (e).

Surface scratches observed here were naturally formed by the movement of the mechanical rolling wheel. Instead of ideal parallel line, scratches observed by 5000$\times$ SEM were discontinuous and malposed, as shown in the inset of Fig. 4. To simplify the analysis, an approximate Mach–Zehnder interferometer (MZI) model was proposed. In Fig. 4, parts of light transmitted in the core was excited into the cladding by the first scratch and then re-coupled back into the core region by the next one, resulting in the interference between the core and cladding modes. This phenomenon is similar to the interference of two cascaded long period fiber gratings [12], [13]. For SPF fabricated by coarse abrasive, high contrast sinusoid interference fringe can be achieved because the surface scratches then formed are small in number and large enough to excite mainly one cladding mode to interfere with the core mode. Although, for smoother SPF by fine abrasive, vast tiny scratches lead to a more complicated multiple interference and then generate the irregular spectrum shown in Fig. 3(f). Beside high contrast interference fringe, insertion loss is another factor need to be optimized. Insertion loss existing in spectrum is mainly caused by the surface scattering of scratches. For SPF1 and SPF2 fabricated by 800 or 1500-mesh coarse abrasive, the insertion loss is about 10 $\sim$ 20 dB. Although, for SPF3 fabricated by fine 3000-mesh abrasive, the insertion loss is somehow above 30 dB due to the contribution of vast tiny scratches to surface scattering. Thus, to realize a higher contrast interference fringe as well as a lower insertion loss, the 800 or 1500-mesh coarse abrasive is a good choice in fabrication.

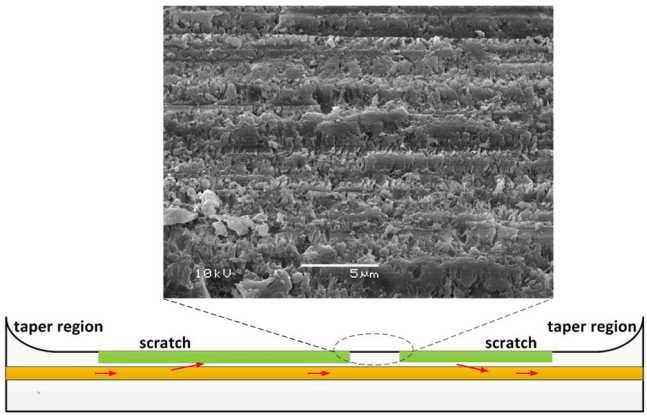

Fig. 4. View of the discontinuous scratches taken by 5000X SEM, and the approximate MZI model for the rough SPF with discontinuous scratches. Yellow: fiber core; white: cladding; green: surface scratches.

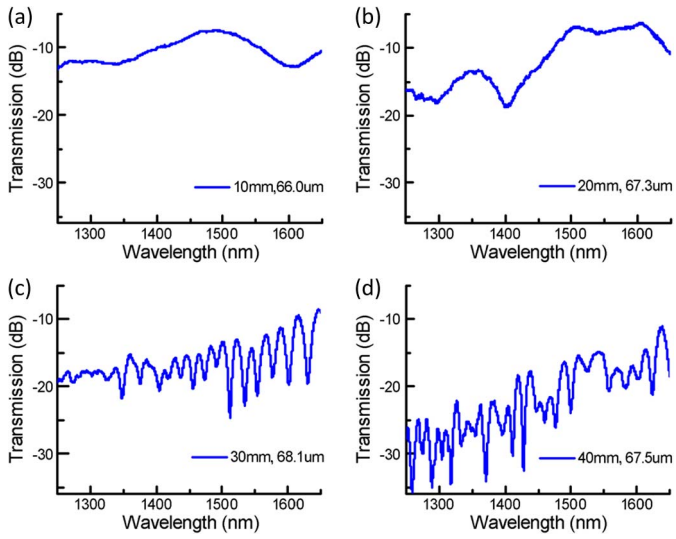

Fig. 5. Transmission profile of four SPFs with different polished lengths of (a) 10 mm, (b) 20 mm, (c) 30 mm, and (d) 40 mm. All SPFs were fabricated by 800-mesh abrasive paper, with the remaining fiber thickness of 67.0, 67.3, 68.1, and 67.5 μm, respectively.

To optimize the polished length of rough SPF, another four SPFs with polished length of 10, 20, 30, and 40 mm were fabricated all by 800-mesh abrasive paper respectively. As shown in Fig. 5(c) and (d), similarly sinusoid interference fringes with contrast ratio around 10 dB were observed in the 30 and 40 mm SPF. Whereas for another two shorter SPFs with polished length of 10 and 20 mm shown in Fig. 5(a) and (b), interference patterns were too weak to figure out. For SPFs all fabricated by 800-mesh abrasive, length of scratches is mainly determined by the rolling movement of mechanical wheel. Statistically, SPF with long polished length is tend to form the cascade MZI structure shown in Fig. 4, ensuring a enhanced MZI interference profile with higher contrast. However, longer polished length also contributes to a large optical path difference, resulting in a more dense resonance dips and higher insertion loss. As compared Fig. 5(d) with Fig. 5(c), the resonance dips of 40 mm-SPF were more crowded than the 30 mm-SPF, and also with higher loss exist in the Fig. 5(d). Therefore, there is a upper limitation for polished length. Empirically, the polished length of the rough-SPF sensor was controlled within 30 to 40 mm in our experiment.

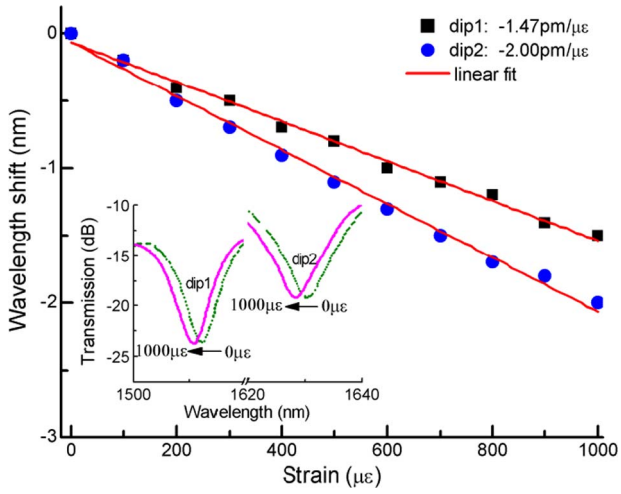

Fig. 6. Wavelength shifts of Dip1 and Dip2 in SPF1's interference fringe in Fig. 3(d), when tensile strain increases from 0 to 1000 $\mu\varepsilon$ with a step of 100 $\mu\varepsilon$.

4. Strain and Temperature Responses

SPF1 illustrated in Fig. 3(a) was chose to investigate the responses of rough SPF to tensile strain and temperature as example. For strain measurement, one end of SPF1 was fixed and another end was attached to a translation stage with a resolution of 10 μm [14]. A tensile strain was applied to SPF1 by moving the translation stage away from the fixed one. The total length of the stretched fiber was 100 mm. Dip1 and Dip2 illustrated in Fig. 3(d) were measured with the increased tensile strain from 0 to 1000 $\mu\varepsilon$ with a step of 100 $\mu\varepsilon$. As the strain applied to the SPF, the difference between the effective refractive index of core and cladding mode changed due to the elasto-optical effect, and the geometry of SPF also deform slightly. As shown in Fig. 6(a), resonant wavelengths of Dip1 and Dip2 around 1512 nm and 1630 nm shift linearly toward a shorter wavelength, which was mainly caused by the elasto-optical effect, with sensitivity of $K_{s1} = -1.47$ pm/$\mu\varepsilon$ and $K_{s2} = -2.00$ pm/$\mu\varepsilon$, respectively.

A column oven (LCO 102, ECOM) with a temperature resolution of 0.1 °C was employed to investigate the thermal response of SPF1 by means of heating it from 30 to 100 °C with a step of 10 °C [15]. At each step, the temperature was stabilized at the target values for 10 min before the spectrum recorded. As shown in Fig. 7, while temperature rose, Dip1 and Dip2 around 1512 nm and 1630 nm shifted linearly toward a longer wavelength due to the thermo-optic effect of the fiber, with sensitivity of $K_{T1} = 25.32$ pm/°C and $K_{T2} = 29.37$ pm/°C respectively.

Assuming the wavelength shift induced by strain and temperature approximated as $y = Kx + b$, where K is expressed as the independent temperature sensitivity K_{T1} and K_{T2}, or strain sensitivity K_{s1} and K_{s2} at each attenuation dips. Combined with the wavelength shift of the two dips $\Delta\lambda 1$ and $\Delta\lambda 2$, the change of strain and temperature ΔS and ΔT can be given by the coefficient matrix below [16], [17]

$$\begin{bmatrix} \Delta S \\ \Delta T \end{bmatrix} = \begin{bmatrix} \kappa_{S1} & \kappa_{T1} \\ \kappa_{S2} & \kappa_{T2} \end{bmatrix}^{-1} \begin{bmatrix} \Delta\lambda_1 \\ \Delta\lambda_2 \end{bmatrix} = \begin{bmatrix} -1.47 & 25.32 \\ -2.00 & 29.37 \end{bmatrix}^{-1} \begin{bmatrix} \Delta\lambda_1 \\ \Delta\lambda_2 \end{bmatrix}.$$

5. Conclusion

In summary, the rough SPF with macro scratches on the polished surface can be directly used to develop a promising sensing device. The cladding modes induced by scratches re-couple back into the fiber core and interfere with the core mode, thus Mach–Zehnder interference pattern occur in the transmission spectrum. In order to achieve SPFs with high interference fringe

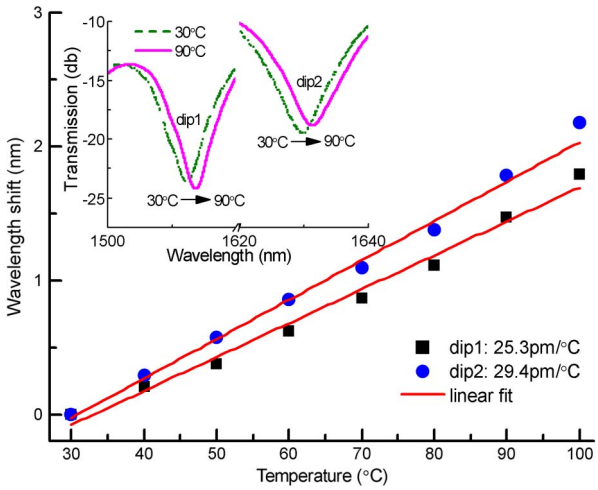

Fig. 7. Wavelength shift of Dip1 and Dip2 in SPF1's interference fringe in Fig. 3(d) when temperature rose from 30 to 100 °C with a step of 10 °C.

contrast ratio above 10 dB, 800-mesh or 1500-mesh coarse abrasive paper was employed, the remaining thickness of the SPF should be controlled between 66 to 68 μm, and polished length should be from 30 to 40 mm. The rough SPF-based sensor exhibited linear response to strain and temperature with sensitivity up to -2.00 pm/μm and 29.37 pm/°C, respectively, which can be used to realize simultaneous strain and temperature measurement. Aiming at the convenient and low-cost sensor application, more other evanescent fiber sensor based on the proposed rough SPF would be researched in next work.

References

[1] Q. L. Bao *et al.*, "Broadband graphene polarizer," *Nat. Photon.*, vol. 5, no. 7, pp. 411–415, 2011.
[2] V. K. S. Hsiao, Z. Li, Z. Chen, P. C. Peng, and J. Y. Tang, "Optically controllable side-polished fiber attenuator with photoresponsive liquid crystal overlay," *Opt. Exp.*, vol. 17, no. 22, pp. 19 988–19 995, 2009.
[3] J. Koo and J. H. Lee, "Passive Q-switching of a fiber laser using a side-polished birefringent fiber with index matching gel spread on the flat side," *Appl. Phys. B*, vol. 112, no. 1, pp. 61–65, Aug. 2013.
[4] N. K. Chen and S. Chi, "Wideband tunable fiber short-pass filter based on side-polished fiber with dispersive polymer overlay," *Opt. Lett.*, vol. 29, no. 19, pp. 2219–2221, Oct. 2004.
[5] S. M. Tseng and C. L. Chen, "Side-polished fibers," *Appl. Opt.*, vol. 31, no. 18, pp. 3438–3447, Jun. 1992.
[6] C. D. Hussey and J. D. Minelly, "Optical fiber polishing with a motor-driven polishing wheel," *Electron. Lett.*, vol. 24, no. 13, pp. 805–807, Jun. 1988.
[7] M. J. F. Digonnet, J. R. Feth, and L. F. Stokes, "Measurement of the core proximity in polished fiber substrates and couplers," *Opt. Lett.*, vol. 10, no. 9, pp. 463–465, Sep. 1985.
[8] O. Leminger and R. Zengerle, "Determination of the variable core-to-surface spacing of single-mode fiber-coupler blocks," *Opt. Lett.*, vol. 12, no. 3, pp. 211–213, Mar. 1987.
[9] Y. X. Zhang, L. Wang, and Z. H. Liu, "The polishing detection method of side-polished fiber," in *Proc. SPIE, Int. Conf. Opt. Instrum. Technol.*, 2011, vol. 8202, Art. ID. 820211.
[10] A. K. Das, M. A. Mondal, A. Mukherjee, and A. K. Mandal, "Automatic determination of the remaining cladding thickness of a single-mode fiber half-coupler," *Opt. Lett.*, vol. 19, no. 6, pp. 384–386, Mar. 1994.
[11] M. H. Cordaro, D. L. Rode, T. S. Barry, and R. R. Krchnavek, "Precision fabrication of D-shaped single-mode optical fibers by in-situ monitoring," *J. Lightw. Technol.*, vol. 12, no. 9, pp. 1524–1531, Sep. 1994.
[12] Y. P. Wang, J. P. Chen, and Y. J. Rao, "Torsion characteristics of long period fiber gratings induced by high frequency CO2 laser pulses," *J. Opt. Soc. Amer. B Opt. Phys.*, vol. 22, no. 6, pp. 1167–1172, Jun. 2005.
[13] X. J. Gu, "Wavelength-division multiplexing isolation fiber filter and light source using cascaded long period fiber gratings," *Opt. Lett.*, vol. 23, no. 7, pp. 509–510, Apr. 1998.
[14] Y. P. Wang, "Review of long period fiber gratings written by CO2 laser," *J. Appl. Phys.*, vol. 108, no. 8, 2010, Art. ID. 081101.
[15] Y. P. Wang *et al.*, "Temperature-controlled transformation in fiber types of fluid-filled photonic crystal fibers and applications," *Opt. Lett.*, vol. 35, no. 1, pp. 88–90, Jan. 2010.
[16] J. Zhou *et al.*, "Simultaneous measurement of strain and temperature by employing fiber Mach–Zehnder interferometer," *Opt. Exp.*, vol. 22, no. 2, pp. 1680–1686, Jan. 2014.
[17] T. Zhu, Y. J. Rao, and Q. J. Mo, "Simultaneous measurement of refractive index and temperature using a single ultra-long-period fiber grating," *IEEE Photon. Technol. Lett.*, vol. 17, no. 12, pp. 2700–2702, Dec. 2005.